Minimum Drag Power-Law Shapes for Rarefied Flow

D. S. Bowman* and Mark J. Lewis†
University of Maryland, College Park, Maryland 20742

SPACE missions that will involve upper atmosphere penetration have led to a recent interest in minimum-drag rarefied-flow aerodynamic shapes. Though there is an extensive body of literature on minimum-drag shapes using continuum assumptions, comparatively little attention has been focused on performance in the large-Knudsen-number regime. Carter[1] determined minimum-drag shapes for missile nose cones in rarefied flow using kinetic theory. Three separate conditions were explored: specular reflection from a smooth surface, specular reflection from a rough surface, and diffuse reflection from a smooth surface. Each minimization assumed that thermal velocity was negligible. The calculus of variations was used to produce the following ordinary differential equations[1]:

$$y_{xx} = \begin{cases} -\left(\dfrac{y_x^2}{y}\right)\left(\dfrac{y_x^2+1}{3-y_x^2}\right), & \text{specular} \\ -\left(\dfrac{y_x^2}{y}\right)\left[\dfrac{\left(1+y_x^2\right)^3-\epsilon\left(1-y_x^4\right)}{\left(3-y_x^2\right)\left(1+y_x^2\right)^2+\epsilon\left(2-6y_x^2\right)}\right], & \text{specular/rough surfaces} \\ -\left(\dfrac{y_x^2}{y}\right)\left(\dfrac{y_x^2+1}{2-y_x^2}\right), & \text{diffuse} \end{cases} \tag{1}$$

where y_x is the first derivative of y with respect to x and ϵ is the positive difference between the reflection and incidence angle. Though the specular and diffuse formulations appear similar, they are in fact unique. Clearly, the minimum-drag shape is dependent on the nature of the gas-surface interaction, which is highly specific to gas species and surface material, and is in general poorly characterized. The specular equation for rough surfaces collapses to the smooth specular equation in the limit $\epsilon \to 0$.

Aerodynamic Model

The goal of the present work has been to reexamine minimum-drag geometries in rarefied flow using more modern computational techniques, with an aerodynamic model that accounts for thermal velocity effects that are important at shallow impingement angles. Since Carter's initial work, numerical techniques have become increasingly available for the calculation of forces in a rarefied flow, including direct simulation, which seeks to model each flow molecule statistically.[2] For practical numerical optimization analytical solutions for the surface forces are still useful for the reduction of computational time and the understanding of underlying physics.

Drag per unit surface area is given generically by

$$\frac{D}{A} = \left[\frac{\mathrm{d}(mV)}{\mathrm{d}t}\right]_{\text{in}} - \left[\frac{\mathrm{d}(mV)}{\mathrm{d}t}\right]_{\text{out}} \cos(\theta+\theta') \tag{2}$$

where the angle definitions are represented in Fig. 1 and m and V are particle mass and velocity, respectively. The impingement rate

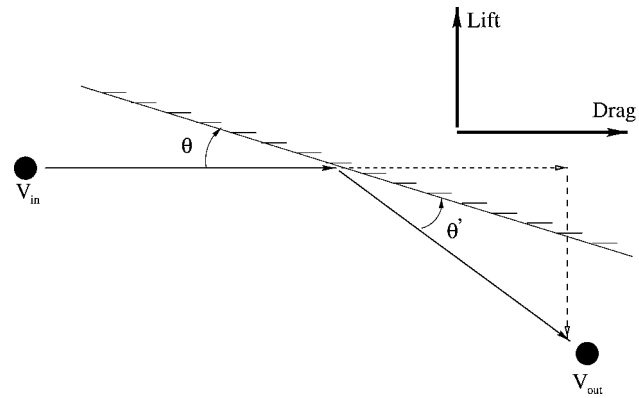

Fig. 1 Physical representation of aerodynamic model.

of Maxwellian particles striking unit area per unit time caused by thermal velocity is given by $I_n = n\bar{c}/4$, where $\bar{c}$ is the average thermal speed and n is the number density.[3] The total flux should properly be calculated by construction of a velocity distribution function, which is biased to the freestream, but this approach yields difficult solutions for all but a few specialized gas-surface assumptions. At typical orbital velocities thermal velocity is approximately an order of magnitude smaller than freestream ($V_{\text{in}} \gg \bar{c}$). Under these conditions, flux can be simplified by linearly summing the thermal and freestream flux:

$$I_m = \rho(V_{\text{in}} \sin\theta + \bar{c}/4) \tag{3}$$

where ρ is the mass density and $\sin\theta$ is the unit capture area of a surface inclined at angle θ to the flow. The effect of thermal impingement is most significant at surface angles smaller than $\sin^{-1}(\bar{c}/4V_{\text{in}})$.

Gas-Surface Interactions

The results of gas-surface interaction must be parameterized in order to characterize the rebound momentum. The range of possible reflection solutions is bracketed between complete accommodation and perfectly specular reflection. The most likely surface interaction will be somewhere in between these limits, with some loss of average momentum and energy exchange, as well as some degree of diffuse flux distribution. Completely diffuse reflections can be thought of as the outgassing of a particle, which hit at some previous time and stuck for a while. The velocity of the particle is therefore, at most, only mildly related to the incoming particle velocity.[2] Previous work has reported that the scattering pattern of a diffuse reflection is, on a limited scale, proportional to a polarly plotted trigonometric distribution, which is symmetric about the surface normal.[4,5] This distribution, which has been used in Monte Carlo simulation schemes,[6] is shown in Fig. 2. Various experimental efforts have shown reflection patterns with some degree of diffusive distribution. This distribution has been added to the present solution as a parametrically specified function.

In specular flow Eq. (2) is written as

$$(D/A)|_{\text{spec}} = I_m V_{\text{in}}[1 - \cos(2\theta)] \tag{4}$$

With diffuse reflections the momentum flux of the integrated reflection pattern is equivalent to a rebound normal to the surface, with

Received 21 June 2001; revision received 7 February 2002; accepted for publication 13 February 2002.

*Graduate Research Assistant, Department of Aerospace Engineering; dsbowman@eng.umd.edu. Student Member AIAA.

†Professor, Department of Aerospace Engineering; lewis@eng.umd.edu. Associate Fellow AIAA.

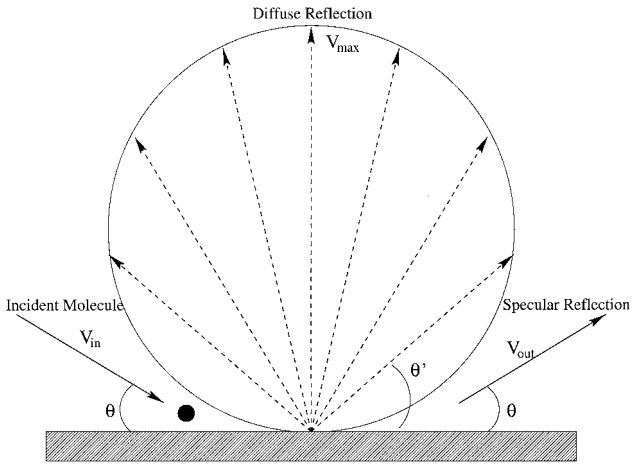

Fig. 2 Cosine law representation of the diffuse reflection possibilities from Ref. 6.

an "effective" velocity that is $\frac{2}{3}$ the maximum velocity of rebound; this is caused by tangential velocity components:

$$(D/A)|_{\text{diff}} = I_m V_{\text{in}}\left[1 - \tfrac{2}{3}\sin\theta'\cos(\theta+\theta')\right] \tag{5}$$

To match the Carter solution, the diffuse reflection is restricted to having only a normal component ($\theta' = \pi/2$), which means that there are no tangential velocity components upon leaving the surface. This represents the special case of particles having no memory of their original momentum when they leave the surface. In reality this is an oversimplification, as some fraction of tangential momentum is typically retained. Making use of a trigonometric identity, Eq. (5) becomes

$$(D/A)|_{\text{diff}} = I_m\ V_{\text{in}}\left(1 + \tfrac{2}{3}\sin\theta\right) \tag{6}$$

The complete drag equation minimized here has been formed from a linear combination of Eqs. (4) and (6):

$$(D/A)|_{\text{complete}} = \xi(D/A)|_{\text{spec}} + (1-\xi)(D/A)|_{\text{diff}} \tag{7}$$

The coefficient ξ is used to determine the percent of specular reflection during a simulation. This equation can be easily employed in drag calculations of simple shapes.

Minimum-Drag Solution

Minimum-drag solutions can be sought in the class of power-law axisymmetric bodies described by

$$\bar{y} = \tau\bar{x}^m \tag{8}$$

where $\bar{y}$ and $\bar{x}$ are radial and axial dimensions, respectively, normalized by the body length l and τ is the slenderness ratio (that is, ratio of base radius to body length). Equation (7) is rewritten in sine terms by making use of the cosine double angle formulations:

$$D/A = \rho V^2(\sin\theta + 1/4s)\left\{1 + \left[(1-\xi)\tfrac{2}{3}\sin\theta + \xi(2\sin^2\theta - 1)\right]\right\} \tag{9}$$

where $s = V/\bar{c}$. The sine of the surface governed by Eq. (8) is

$$\sin\theta = \frac{\tan\theta}{\sqrt{\tan^2\theta + 1}} = \frac{m\tau\bar{x}^{m-1}}{\sqrt{(m\tau)^2\bar{x}^{2m-2} + 1}} \tag{10}$$

The surface area of a body of revolution is given by

$$A = 2\pi\int_{0^+}^{1} \tau\bar{x}^m\sqrt{1 - (m\tau)^2\bar{x}^{2m-2}}\,\mathrm{d}\bar{x} \tag{11}$$

The integral has no solution at $\bar{x} = 0$, and so it is evaluated at 0^+. Calculations on the interval $[0, 0^+]$ assume a cone shape. The total drag on the power-law body is

$$D = 2\pi\int_{0^+}^{1} \frac{D}{A}\tau\bar{x}^m\sqrt{1 - (m\tau)^2\bar{x}^{2m-2}}\,\mathrm{d}\bar{x} \tag{12}$$

Upon algebraic reduction, Eq. (12) is written as

$$D = A\int_{0^+}^{1}\left[B\sin^3\theta + C\sin^2\theta + E\sin\theta + \frac{(1-\xi)}{4s}\right] \times\left(\bar{x}^m\sqrt{1 - (m\tau)^2\bar{x}^{2m-2}}\right)\mathrm{d}\bar{x} \tag{13}$$

where

$$A = 2\pi\tau\rho V^2, \qquad B = 2\xi, \qquad C = \tfrac{2}{3} - (\xi/6s)\xi + \xi/2s$$
$$E = 1 - \xi + (1-\xi)/6s \tag{14}$$

Thus, the drag on the power-law shape is a function of slenderness ratio τ, exponent m, and specular-to-diffuse ratio ξ.

Numerical Minimum-Drag Results

Carter reported solving the ordinary differential equation [ODE; Eq. (1)] for minimum drag numerically using a second-order Euler solution. From this solution Carter provided a table of data points for an example specular minimum-drag solution. In this present work the governing ODE has been solved using a fourth-order Runge–Kutta method. Some discrepancies have been found with the Carter solution, most likely as a result of the improved accuracy of the fourth-order scheme. The Runge–Kutta solution and Carter's reported data are compared in Fig. 3. The numerical solution of the drag ODE is sensitive to the step size (Δx) so that it is not surprising that a more accurate solution is obtained with modern computing resources.

Specular and diffuse solutions obtained with the Runge–Kutta method are provided in Fig. 3. The results are not power-law shapes themselves, but they can be closely fitted with power-law curves whose nonnormalized coefficients are shown on the plot. These curve-fit shapes have been solved for the special case of $\tau \approx 0.1$

Minimum-drag shapes were first solved under conditions of negligible thermal velocity (to match the Carter solution), mass density (ρ) of 6.2E-9 kg/m^3 (approximately an altitude of 130 km), and a spacecraft velocity of 8 km/s. Minimum-drag exponents are plotted for a range of τ in Fig. 4. It is seen that both the specular and diffuse curves vary across a wide range of optimum power-law exponent m. Also, both curves follow a similar trend; as the body becomes less slender (that is, as τ increases), the minimum-drag shape tends to have greater curvature (lower value of m). For $\tau \approx 1.0$ the optimum shapes have similar values of power-law exponent. In this regime the minimum-drag shape is insensitive to the reflection condition, though its performance (that is, magnitude of drag) obviously will be. The very slender Carter shapes for both specular and diffuse conditions (which were presented in Fig. (3) are found in these

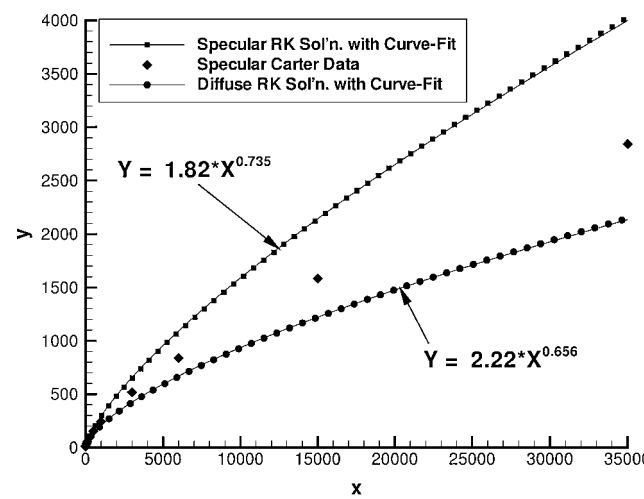

Fig. 3 Solution to the specular and diffuse Carter ODE and curve fits.

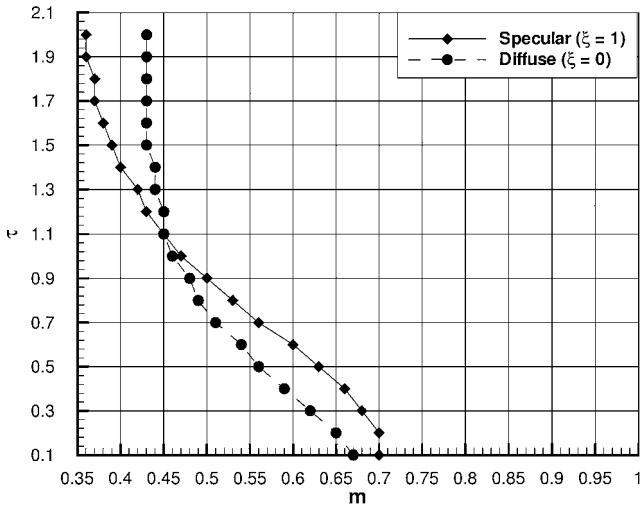

Fig. 4 Minimum-drag power-law coefficients for negligible thermal velocity.

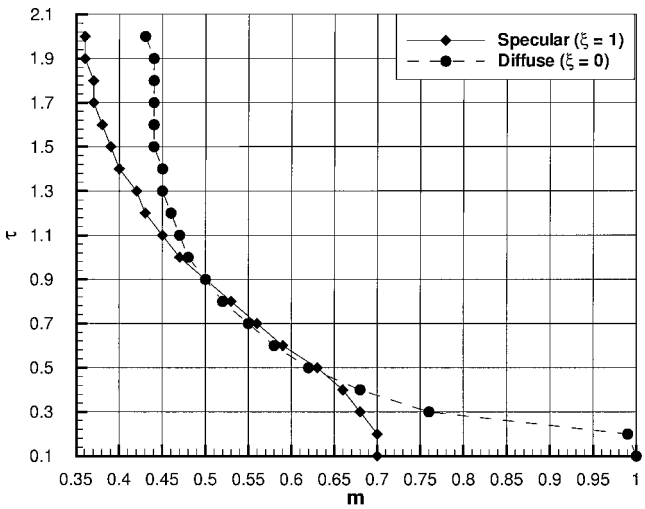

Fig. 5 Minimum-drag power-law coefficients for finite thermal velocity.

curves, as the Carter solution is a subset of this minimum drag power-law solution. These shapes resemble power-law functions with exponents ranging between $\frac{2}{3}$ and $\frac{3}{4}$, quite similar to minimum-drag shapes derived for hypersonic flow under the continuum Newtonian flow assumption of total loss of normal momentum.

Additional calculations were performed with thermal velocity component on the order of one-tenth the spacecraft velocity (which is characteristic for 130-km altitude). Minimum drag coefficients for this condition are shown in Fig. 5. Compared to Fig. 4, the specular curve has essentially no change with the addition of thermal impingement.

Conclusions

Numerical results indicate that the power-law exponent, which corresponds to a minimum-drag body in rarefied flow, is a function of not only the gas-surface interaction model, but the relative magnitude of thermal (that is, random) velocities under realistic orbital conditions. The cases presented include a wide range of practical conditions for an axisymmetric body, although the choice of an optimal shape will obviously depend on the surface material and ambient atmospheric composition. More complicated geometries, including nonaxisymmetric shapes, volume-constrained forms, etc., would have different results and might have to be solved with a completely numerical formulation. In the cases studied, the resulting minimum drag nose geometry under assumption of specular reflection is a weak function of the thermal velocity component. Such a result is to be expected because thermal velocity only influences drag at shallow surface angles, though specular collisions transfer little momentum at shallow angles. In contrast, the exponent for a minimum-drag shape under diffuse reflection was insensitive to the addition of thermal impingement at large τ but significantly affected at $\tau < 0.5$. In this range the optimum nose shape approaches a cone ($m = 1$) because the shallow surface angles receive significant momentum transfer as a result of the thermal velocity. At values of slenderness ratio in the range $0.4 < \tau < 1.0$ with thermal velocity equal to $\frac{1}{10}$ freestream velocity, the mimimum-drag power-law exponent is nearly identical for either specular or diffuse reflection models. This has the very practical benefit that a minimum-drag shape can be selected even though there might be significant uncertainty regarding the nature of gas-surface interactions. The magnitude of drag on that optimal shape will be dependent on the surface interactions.

References

[1]Carter, W. J., "Optimum Nose Shapes for Missiles in the Superaerodynamic Region," *Journal of the Aeronautical Sciences*, Vol. 7, July 1957, pp. 527–532.

[2]Bird, G. A., *Molecular Gas Dynamics and the Direct Simulation of Gas Flows*, Clarendon, New York, 1994, pp. 1–14.

[3]Vincenti, W. G., and Kruger Charles, H. J., *Introduction to Physical Gas Dynamics*, Krieger, Malabar, FL, 1986, pp. 47, 48.

[4]Goodman, F. O., and Wachman, H. Y., *Dynamics of Gas-Surface Scattering*, Academic Press, New York, 1976, pp. 23, 24.

[5]Kuhlthau, A. R., and Bishara, M. N., "On the Nature of the Surface Interaction Between Inert Gas Molecules and Engineering Surfaces," *Rarefied Gas Dynamics*, edited by J. H. de Leeuw, Vol. 2, 1996, pp. 518–535.

[6]Woronowicz, M. S., and Rault, D. F. G., "Cercignani-Lampis-Lord Gas-Surface Interaction Model: Comparisions Between Theory and Simulation," *Journal of Spacecraft and Rockets*, Vol. 31, No. 3, 1994, pp. 532–534.

E. Livne
Associate Editor

Boundary-Layer Instability on Sharp Cone at Mach 3.5 with Controlled Input

T. C. Corke*
University of Notre Dame, Notre Dame, Indiana 46556
D. A. Cavalieri†
Illinois Institute of Technology, Chicago, Illinois 60616
and
E. Matlis‡
University of Notre Dame, Notre Dame, Indiana 46556

Nomenclature

F	=	dimensionless frequency, $2\pi f \nu / U^2$
n	=	oblique wave azimuthal mode number
s	=	azimuthal spacing between actuators
x, y, θ	=	streamwise, wall-normal, and azimuthal directions
λ	=	spanwise wavelength
ψ	=	oblique wave angle

Received 11 January 1999; revision received 4 July 2001; accepted for publication 9 July 2001.

*Clark Professor of Engineering, Center for Flow Physics and Control, Aerospace and Mechanical Engineering Department. Associate Fellow AIAA.

†Graduate Assistant, Mechanical and Aerospace Engineering Department; currently Senior Project Engineer, Bigelow Aerospace, 1899 W. Brooks Avenue, Las Vegas, NV 89032. Member AIAA.

‡Ph.D. Candidate, Center for Flow Physics and Control, Aerospace and Mechanical Engineering Department.